A Double-Layered Elbow Exoskeleton Interface with 3-PRR Planar Parallel Mechanism for Axis Self-Alignment

Mohammad I. Awad[1]†
Health Engineering Innovation Center (HEIC), Khalifa University of Science and Technology, Abu Dhabi, UAE
Khalifa University Center for Autonomous Robotic Systems (KUCARS), Khalifa University of Science and Technology, Abu Dhabi, UAE
Abu Dhabi Campus. PO Box 127788, Abu Dhabi, UAE
mohammad.awad@ku.ac.ae
ASME Membership: ***Professional Member*** (000100639263)

Irfan Hussain †
Khalifa University Center for Autonomous Robotic Systems (KUCARS), Khalifa University of Science and Technology, Abu Dhabi, UAE
Abu Dhabi Campus. PO Box 127788, Abu Dhabi, UAE
irfan.hussain@ku.ac.ae

Shramana Ghosh
Department of Mechanical and Aerospace Engineering
NYU Tandon School of Engineering
Brooklyn, NY, USA Email: sg5760@nyu.edu

Yahya Zweiri
Faculty of Science, Engineering and Computing, Kingston University London, London SW15 3DW, UK;
y.zweiri@kingston.ac.uk
Khalifa University Center for Autonomous Robotic Systems (KUCARS), Khalifa University of Science and Technology, Abu Dhabi, UAE
Abu Dhabi Campus. PO Box 127788, Abu Dhabi, UAE

Dongming Gan[1]
School of Engineering Technology, Purdue University
West Lafayette, IN 47907, US
dgan@purdue.edu
ASME Membership (000100324083)

[1] Corresponding authors information: Mohammad I. Awad (mohammad.awad@ku.ac.ae) and Dongming Gan (dgan@purdue.edu)
† Authors contributed equally to the manuscript

ABSTRACT

Designing a mechanism for elbow self-axis alignment requires the elimination of undesirable joint motion and tissue elasticity. The novelty of this work lies in proposing a double layered interface using a 3-PRR planar parallel mechanism as a solution to the axis alignment problem. 3-PRR planar parallel mechanisms are suitable candidates to solve this as they can span the desired workspace in a relatively compact size. In this paper, we present the modeling, design, prototyping and validation of the double-layered elbow exoskeleton interface for axis self-alignment. The desired workspace for the self-axis alignment mechanism is specified based on the estimated maximum possible misalignment between the exoskeleton joint and the human anatomical elbow joint. Kinematic parameters of the 3-PRR planar mechanism are identified by formulating an optimization problem. The goal is to find the smallest mechanism that can span the specified workspace. The orientation angle of the mechanism's plane addresses the frontal frustum vertex angel of the elbow's joint, while the translational motion allows the translational offsets between the user's elbow and the exoskeleton joint. The designed exoskeleton axis can passively rotate around the frontal plane ±15 degrees and translate along the workspace 30 mm in the frontal plane. Experimental results (quantitative and qualitative) confirmed the capability of the proposed exoskeleton in addressing the complex elbow motion, user's satisfaction and ergonomics.

1. INTRODUCTION

1.1 State of the art.

Stroke is the main cause of long-term impairment which affects the lives of millions of people [1]. Impairment of the upper limb is one of the common post stroke deficits. Almost 85% of the cases, stroke causes hemiparesis resulting in impairment of upper limb. The patients face problems in performing even simple Activity Daily Living (ADL) tasks. In addition, it leads to more expenditures of healthcare resources on continued medical and

social care [2]. In the last two decades, several rehabilitation teams have started to integrate robotic-aided therapies in their rehabilitation projects. Such treatments represent a novel and promising approach in rehabilitation of the post stroke paretic upper limb. The use of robotic devices in rehabilitation can provide high-intensity, repetitive, task-specific, and interactive treatment of the impaired upper limb and can serve as an objective and reliable means of monitoring patient progress [3-5]. Rehabilitation process using robotic devices is being accepted by the heathcare community slowly and even being considered better than manual therapy [6-8]. In literature, several robotic devices ranging from end point manipulators [7, 9-12], cable suspensions [13], and exoskeletons [14-17] have been proposed.

In general, exoskeletons are designed to transfer a controlled amount of power to the user's limb and to monitor its position at the same time [16]. The user's limb is rigidly coupled with the exoskeleton and to avoid any unwanted forces during the motion, the exoskeleton should match the constraints given by the kinematics of the limb.

A major source of user's discomfort in wearing an exoskeleton is caused by the misalignment between the joint axes of the exoskeleton and the anatomical axes of the human joints [16]. This misalignment creates undesirable torques applied by the exoskeleton to force relative translations on the skin, the internal musculoskeletal system, and the trunk, causing discomfort and pain to the user [17]. Several complications that must be addressed to achieve axes alignment between the exoskeleton axes and the human joint axes like the added redundancy, complexity and the variability of the human musculoskeletal system [18].

In human bodies, many joints such as the knee or elbow, are often treated as a simple revolute joint. On the other hand, the motion of these joints is complex and without the use of sophisticated imaging technologies the location of anatomical joint axes cannot be exactly determined from the outside [17]. Several solutions were reported in literature to address the axis alignment issue. One way consists of rectifying the misalignment of axes by not fixing the trunk of the human body, and forcing it to move relative to the exoskeleton to make the required adjustments. This method was applied in some exoskeletons like LEXOS [19] and CADEN-7 [20]. However, this method does not eliminate the possibility of an injury to the user.

Another way to address the misalignment issue is by incorporating additional mechanisms in the exoskeleton. In Stienen et al. [17], the principle of adding an additional mechanism that decouples joint rotations from joint translations which automatically aligns exoskeleton axes to human joint axes was proposed. This principle had been demonstrated by attaching a linear guidance mechanism to the Dampace exoskeleton [21] and a Double Parallelepiped mechanism to the Limpact exoskeleton [22]. The exoskeleton of the European Space Agency [23] added a number of passive links such that the exoskeleton did not require alignment to the human joint axes, yet was able to actuate each DOF of its redundant limb unambiguously and without reaching into singularities. The WREX exoskeleton [24] had additional two-link mechanisms for horizontal shoulder translations. A vertical four-link mechanism that coupled the shoulder elevation rotation of the exoskeleton to its vertical shoulder translation with a single DOF was presented in the ARMin [25]. In NEUROExos [26] a four-degree-of-freedom passive

mechanism, designed by taking into account elbow laxity, was embedded in the exoskeleton and allowed the user's elbow and robot axes to be constantly aligned during movement. In [27], a theoretical treatment of the problem of hyperstaticity in exoskeleton connections was presented. Although the presented method was limited to anthropomorphic exoskeletons, but it clearly addressed the issue of reduced mobility due to the replication of the limb kinematics done by the exoskeleton structure which formed rigid connections with the user's body. They presented a methodology for adding passive DOFs (Degrees of Freedom) to the attachment points of robots to comply with hyperstaticity. Further, kinetostatic analysis in human-robot skeleton as a coupled mechanism was presented in [16], which provided insights about the design of self-aligning mechanisms when the robot did not replicate human body kinematics. Recently, the misalignment problem was addressed in the Full-DOF Hip Exoskeleton [31] by adding a single-DOF passive prismatic joint along each axis (flexion/extension axis, internal/external rotation axis, and abduction/adduction axis). The misalignment of each axis was compensated by the two prismatic joints attached to the other axes. In [44], a novel 4-DoF self-aligning exoskeleton mechanism was proposed for upper limb rehabilitation. In [45], a 5-DoF lightweight Elbow-wrist exoskeleton for forearm fine motion rehabilitation was introduced. A passive prismatic joint was used for addressing the misalignment problem for the elbow. In [46], authors addressed the knee frontal plane misalignment problem by implementing a double-hinge mechanism on the mechanical frame between the rolling knee joint and the proximal calf attachment point. To the best of our knowledge, the state of art is still missing the exploitation of the double

layered parallel mechanism to address the misalignment problem. We exploit the use of a parallel mechanism to solve the axis alignment problem. In general, parallel mechanisms are very suitable in such applications due to their inherent features, e.g. ability to deliver desired workspaces for relatively compact mechanism size, high stiffness, and low inertia of moving parts.

1.2 Contribution

In particular, our main contributions in this paper are following.

1. We present a novel approach to the self-axis alignment problem for an elbow exoskeleton by using a planar parallel mechanism. In particular, a double layered 3-PRR planar mechanism is designed, developed and deployed.
2. The geometric parameters of the 3-PRR planar parallel mechanism are identified by solving an optimization problem using Genetic Algorithms. We determined the smallest mechanism that can cover a specified workspace that represents the possible area of misalignment
3. A 3D-printed elbow exoskeleton prototype was built by attaching the platform of the mechanism to the exoskeleton and the base to the user's arm.
4. We performed quantitative and qualitative experiments to confirm both functional and ergonomics requirements of the device.

The rest of the paper is organized as follows. In section 2, we present the design and development of the passive version of Self-Alignment Elbow Exoskeleton (SAE-Exo) based on the proposed double-layer parallel mechanism. Afterwards, the model, analysis

optimization and the design of the 3-PRR Mechanism is detailed in section 3. In section 4, the quantitative and qualitative experiments conducted to validate the proposed mechanism is reported. Finally, conclusion and future work are presented in section 5.

2. DESIGN AND DEVELOPMENT OF THE SELF-ALIGNMENT ELBOW EXOSKELETON (SAE-EXO)

The SAE-Exo is intended to be a powered elbow exoskeleton for rehabilitation purposes. The current version of the SAE-Exo is passive as the focus at this stage is to evaluate and validate the SAE-Exo features of self-axis alignment. SAE-Exo is composed of a passive 3-PRR planar parallel mechanism and 3D printed elbow joint parts. The CAD model of the SAE-Exo is shown in Fig. 1 and the fabricated model (weight 1.1kg) is shown in Fig. 2. The elbow joint rotates around revolution axis (A_R). The exoskeleton frontal arm's part is a 3D printed link connecting the elbow joint and an arm shim. The exoskeleton upper arm consists of the upper elbow part connected to the platform of the 3-PRR mechanism and a link connecting the base of the 3-PRR mechanism and the upper arm pad. Motion of the 3-PRR will address the translation of the elbow arm along the frontal plane and the orientation along the frustum angle of the frontal plane (β_f).

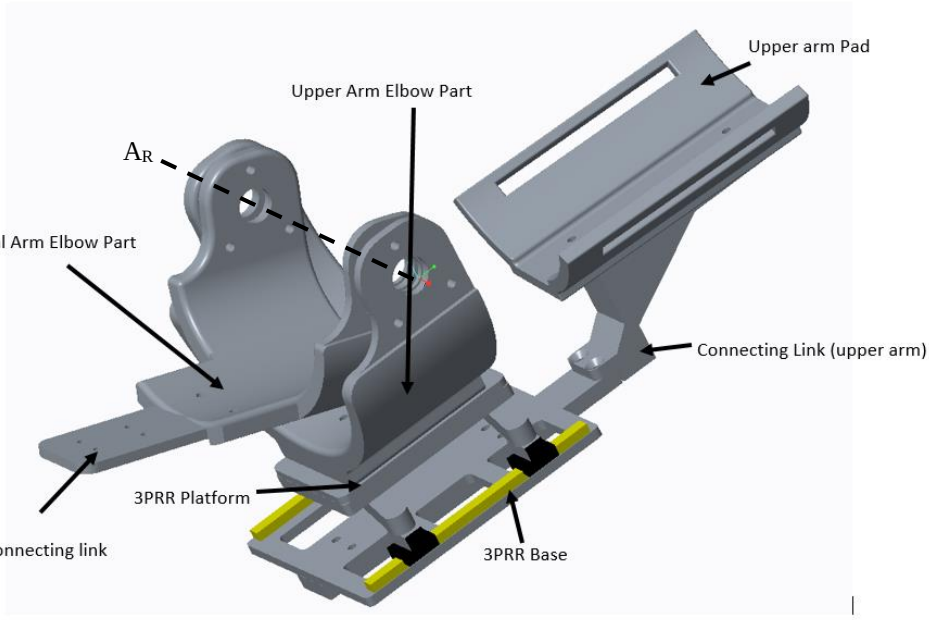

Figure 1: CAD model of the SAE-Exo

Figure 2: The prototype of the proposed exoskeleton with the 3-PRR planar parallel mechanism for axis alignment

3. The 3-PRR Passive Planar Parallel Mechanism

3.1 Passive motion requirement in human elbow joint

For elbow exoskeletons, the exoskeleton's joint can be decoupled from the human joint using a planar linkage [28], [29]. It should be noted that without a mounted human arm, the additional passive mechanisms create an underdetermined system. However, with the decoupled joint mounted on a human arm, the passive segments are fully constrained by the kinematics of the human joint [17]. From Orthopedic point of view, a human elbow acts like a 'loose hinge joint' [26], [28], [30]. During the flexion-extension motion, the elbow rotation axis is not fixed. It traces the surface of a double quasi-conic frustum with an elliptical cross section [29, 30] (see Fig 3). The position of the joint axis not only varies among different individuals, but also for the same person under different conditions like active or passive motion of the joint. In particular, the frustum vertex angles β_f on the frontal plane, and β_f on the horizontal plane, assume a maximum value of about 10° and 6°, respectively [26]. Moreover, the elbow average rotation axis over a full flexion–extension task forms an angle of 80–92◦ with the humerus longitudinal axis A_H (see, Fig. 3) onto the frontal plane, and an angle of ±5◦ with the medial-lateral anatomic axis A_{ML} onto the horizontal plane [26].

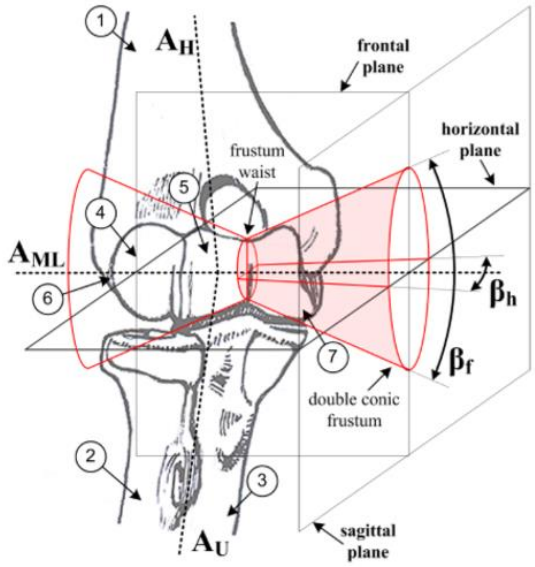

Figure 3: Anatomy of the human elbow. (1) Humerus. (2) Radius. (3) Ulna. (4) Capitellum. (5) Trochlea. (6) Lateral facet of capitellum. (7) Lateral facet of trochlea. AH is the humerus longitudinal axis, AU is the ulna longitudinal axis, AML is the anatomical medial-lateral axis passing from the capitellum center to the trochlear center [17], and βh andβf are the frustum vertex angles, respectively, on the horizontal and frontal planes (adopted from [26, 33]) .

Designing a mechanism for elbow self-axis alignment requires elimination of undesirable motion in the front plane (translational or rotation) or the translational motion due to the tissue elasticity. Planar parallel mechanisms are a candidate solution that can address such requirements. In addition, they have other desirable features such as better stiffness compared with their serial counterparts, and the minimal inertia of moving parts [34]. Based on the requirements mentioned above, a planar parallel mechanism that involves positioning and orientation on the plane with high stiffness is needed. Thus, a 3-PRR mechanism is selected to address these requirements.

The design problem for such mechanisms can be formulated in two ways. The first way is through synthesizing a mechanism whose workspace encapsulates a desired

workspace. The other way is to find the geometry of a mechanism that maximizes the workspace [36]. In [35], we started to explore the possibility of using parallel mechanism for axis alignment problem. In particular, we presented our preliminary study on theoretical development of proposing an optimization methodology to obtain a design candidate for a completely passive parallel self-aligning mechanism. The aim was to find the suitable mechanism that can provide constant corrective action in case of misalignment between the joint axis of an exoskeleton and its user. This method is used to synthesize a mechanism workspace that closely resembles the desired or prescribed workspace. The main advantage of this method is that it produces a compact mechanism that fits the desired application. In this work, we briefly recall our previous theoretical study and further extend our work for modeling, design, prototyping, and validation of a double-layered elbow exoskeleton interface for self-axis alignment.

3.2 MODEL, ANALYSIS AND DESIGN OF THE 3-PRR WITH PARALLEL PRISMATIC JOINTS

In this subsection, modeling, analysis, and design of the 3-PRR passive mechanism is presented. The 3-PRR topology was first presented by Gosselin, Lemieux and Merlet [34]. In their work, they introduced the kinematic analysis of the mechanism and also generated the workspace of the new mechanism based on its geometry giving a description of the boundaries of its workspace. The general architecture and kinematics model of the 3-PRR planar parallel mechanism is illustrated in Appendix A. This will be the basis for the proposed 3-PRR mechanism that has a specific architecture with parallel

prismatic joints. In the following subsections, the architecture, inverse kinematics, and Jacobian of the proposed 3-PRR mechanism are discussed.

3.2.1 The Specific Architecture

Having studied the general 3-PRR planar parallel mechanism (Appendix A), we now adapt the geometry of the platform for the purpose of aligning the axes of an exoskeleton with the human anatomical joint axis. The most commonly used and studied geometry of the 3-PRR planar platform consists of a triangular (equilateral or isosceles) base platform connected to a similar triangular moving platform through three PRR chains. In a mechanism intended to facilitate alignment between the exoskeleton axes and human joint axes, the base and moving platforms have to be connected to a sheath and the exoskeleton respectively. Considering the human arm's cylindric geometry and ergonomic needs, a rectangular architecture for the platforms will have compact dimensions and confer good stability to the mechanism as it will have a large surface area in contact with the objects it attaches to. A line sketch and a CAD model of the proposed architecture is shown in Fig. 4, in which the three prismatic joints are parallel and two (limb 1 and 3) of them are in line. Two of the fixed pivots (A_1, A_3) and moving pivots (C_1,C_3) lie on the same side of the base and moving platforms respectively while the remaining pivots (A_2/C_2) sit on the opposite side. This provides a compact design and a free and large translation motion along the y-axis which is the main free motion along the upper arm.

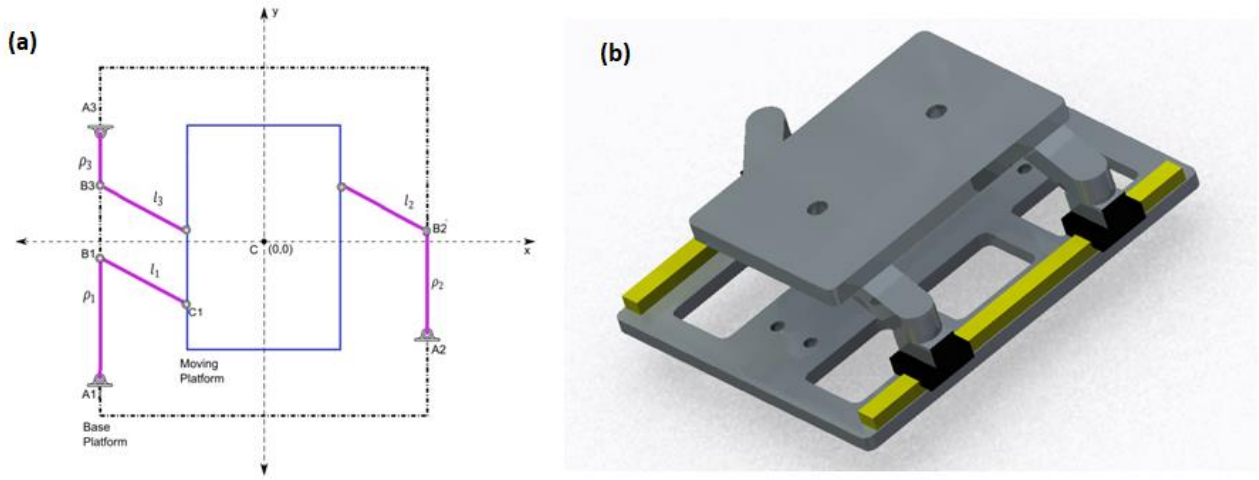

Figure 4: (a) Scheme of the realized 3-PRR mechanism (b) CAD Model of the 3PRR mechanism

3.2.2 Inverse Kinematics and Workspace of the 3-PRR with Parallel Prismatic Joints

The angles made by the prismatic joint axes at the base are constant as $\alpha_1 = 90^0$, $\alpha_2 = 90^0$, $\alpha_3 = -90^0$. By substituting them into the general model in Appendix A, the inverse kinematics solution can be obtained from Eq. (A4) as:

$$\begin{cases} \rho_i = (y_{Ci} - y_{Ai}) \pm \sqrt{{l_i}^2 - (x_{Ci} - x_{Ai})^2} \quad (i = 1,2) \\ \rho_3 = (-y_{C3} + y_{A3}) \pm \sqrt{{l_3}^2 - (x_{C3} - x_{A3})^2} \end{cases} \tag{1}$$

Thus, the proposed 3-*PRR* parallel mechanism has a simpler inverse kinematics than the general structure and it will be used for further analysis including the workspace modeling.

To demonstrate the workspace properties of the new 3-*PRR* parallel mechanism, a geometric method is used in this section. Several types of workspace regions can be defined such as the reachable workspace, the constant orientation workspace, the dexterous workspace, and the total orientation workspace [19]. We rely on the constant

orientation workspace for this work. Hence, we look at the workspace of the mechanism as the region in plane that can be traversed by a given point on the moving platform, for a given orientation of the moving frame. To find the general workspace, this calculation can be repeated for all achievable orientations of the moving platform. The workspace of the 3-PRR platform can be expressed as the intersection of three regions, which are simply the regions that point *C* can attain when considering the constraints on each of the legs of the mechanism independently, for a constant orientation as shown in Fig. 5. The region which can be attained by point *C* with a constant orientation of the platform and considering the constraints on only one leg is bounded by two parallel line segments connected in their ends by two half-circles [25]. The line segments can be expressed parametrically in terms of λ as:

$$x = x_{Ai} - (x'_{Ci}\cos(\emptyset) - y'_{Ci}\sin(\emptyset)) \pm l_i \sin(\alpha_i) + \lambda_i \cos(\alpha_i) \quad (2)$$

$$x = y_{Ai} - (x'_{Ci}\sin(\emptyset) + y'_{Ci}\cos(\emptyset)) \pm l_i \cos(\alpha_i) + \lambda_i \sin(\alpha_i) \quad (3)$$

$$\rho_{i\,min} \leq \lambda_i \leq \rho_{i\,max} \text{ where i=1,2,3} \quad (4)$$

The two have circles can be expressed in terms of parameter ψ as:

Half-circle 1:

$$x = x_{Ai} + \rho_{i\,min}\cos(\alpha_i) - (x'_{Ci}\cos(\emptyset) - y'_{Ci}\sin(\emptyset)) + l_i \cos(\psi_i) \quad (5)$$

$$x = y_{Ai} + \rho_{i\,min}\sin(\alpha_i) - (x'_{Ci}\sin(\emptyset) + y'_{Ci}\cos(\emptyset)) + l_i \sin(\psi_i) \quad (6)$$

$$\alpha_i - \frac{3\pi}{2} \leq \psi_i \leq \alpha_i - \frac{\pi}{2} \text{ where i=1,2,3} \quad (7)$$

Half-circle 2:

$$x = x_{Ai} + \rho_{i\,max}\cos(\alpha_i) - (x'_{Ci}\cos(\emptyset) - y'_{Ci}\sin(\emptyset)) + l_i\cos(\psi_i) \quad (8)$$

$$x = y_{Ai} + \rho_{i\,max}\sin(\alpha_i) - (x'_{Ci}\sin(\emptyset) + y'_{Ci}\cos(\emptyset)) + l_i\sin(\psi_i) \quad (9)$$

$$\alpha_i - \frac{\pi}{2} \leq \psi_i \leq \alpha_i + \frac{\pi}{2} \text{ where i=1,2,3} \quad (10)$$

The ranges illustrated in equations 7 and 10 are valid if and only if

$$\frac{\rho_{i\,max} - \rho_{i\,min}}{2} > l_i \quad (11)$$

If this condition in equation 11 is not satisfied, the ranges in equations 7 and 10 will become:

$$-\pi \leq \psi_i \leq \pi \text{ where i=1,2,3} \quad (12)$$

Based on the above equations, the workspace of the new 3-PRR parallel mechanism can be illustrated as in Fig.5 for different constant orientations of which the workspace is significantly different. It also can be seen that the common area among the three figures lies in the ranges of x = {-21, -3} and y={-25, 10}.

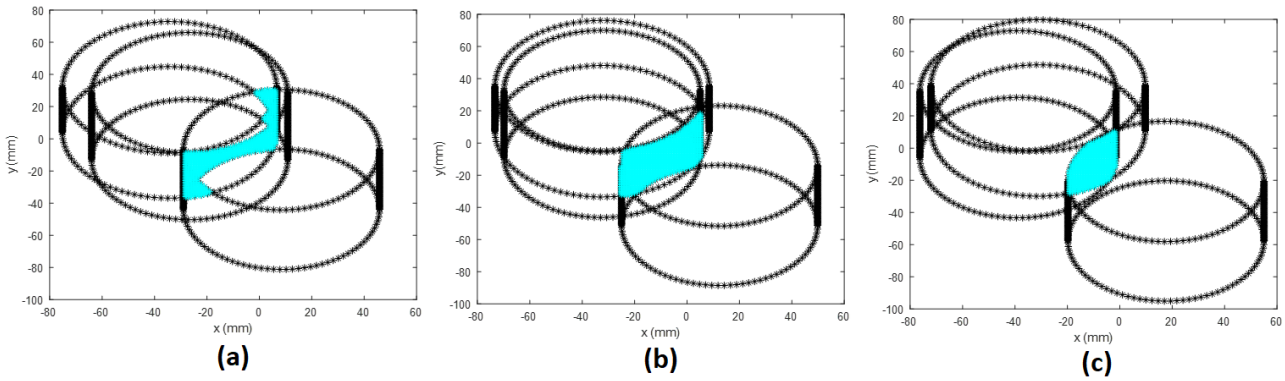

Figure 5 Sample constant orientation workspace (area covered in cyan) of the 3-PRR (a) φ=-10°, (b) φ=0°, (c) φ=10°

3.2.3 Jacobian-based Kinematics Performance and Singularity Analysis

One of the commonly used methods to analyze the kinematic performance of parallel mechanisms is the Jacobian-based method. The determinant of the Jacobian can be used to find singularity configurations and the condition number represents the kinematic mapping of its performance at any given configuration in the workspace. Based on the geometric setup in Fig.4(a), the link C_iB_i has a constant length as:

$$(\boldsymbol{C}_i - \boldsymbol{B}_i)^{\boldsymbol{T}}.(\boldsymbol{C}_i - \boldsymbol{B}_i) = l_i^2 \tag{13}$$

which can be specified as:

$$(\mathbf{R} * \boldsymbol{C}_i' + \boldsymbol{P} - \rho_i * \boldsymbol{u}_i)^{\boldsymbol{T}}.(\mathbf{R} * \boldsymbol{C}_i' + \boldsymbol{P} - \rho_i * \boldsymbol{u}_i) = l_i^2 \tag{14}$$

where $\boldsymbol{P}=[x_c, y_c]^T$ is the translation vector between the centers of the coordinate frames, **R** is the rotation matrix between the platform coordinate and the base coordinate as:

$$\mathbf{R} = \begin{bmatrix} cos\emptyset & -sin\emptyset \\ sin\emptyset & cos\emptyset \end{bmatrix}$$

$\boldsymbol{u}_i$ are the unit vectors of the prismatic joint directions with $\boldsymbol{u}_1 = \boldsymbol{u}_2 = -\boldsymbol{u}_3 = [0, 1]^T$ along the y-axis direction.

By taking the derivative of Eq.14 and combine the three limb equations in matrix format, there is:

$$\begin{bmatrix} \boldsymbol{w}_1^T.\mathbf{R}_1 * \boldsymbol{C}_1' & \boldsymbol{w}_1^T \\ \boldsymbol{w}_2^T.\mathbf{R}_1 * \boldsymbol{C}_2' & \boldsymbol{w}_2^T \\ \boldsymbol{w}_3^T.\mathbf{R}_1 * \boldsymbol{C}_3' & \boldsymbol{w}_3^T \end{bmatrix} \begin{bmatrix} \dot{\emptyset} \\ \dot{x} \\ \dot{y} \end{bmatrix} = \begin{bmatrix} \boldsymbol{w}_1^T.\boldsymbol{u}_1 & 0 & 0 \\ 0 & \boldsymbol{w}_2^T.\boldsymbol{u}_2 & 0 \\ 0 & 0 & \boldsymbol{w}_3^T.\boldsymbol{u}_3 \end{bmatrix} \begin{bmatrix} \dot{\rho}_1 \\ \dot{\rho}_2 \\ \dot{\rho}_3 \end{bmatrix} \tag{15}$$

where $\boldsymbol{w}_i$ is the unit vector of the link C_iB_i, and:

$$\mathbf{R_1} = \begin{bmatrix} -sin\emptyset & -cos\emptyset \\ cos\emptyset & -sin\emptyset \end{bmatrix}$$

Eq. (15) can be represented as:

$$\mathbf{J}_A \begin{bmatrix} \dot{\emptyset} \\ \dot{x} \\ \dot{y} \end{bmatrix} = \mathbf{J}_B \begin{bmatrix} \dot{\rho}_1 \\ \dot{\rho}_2 \\ \dot{\rho}_3 \end{bmatrix} \tag{16}$$

where $\mathbf{J}_A$ and $\mathbf{J}_B$ are the Jacobian matrices.

When det($\mathbf{J}_B$)=0, the mechanism is in actuation singularity and one of the limbs has $\boldsymbol{w}_i^T . \boldsymbol{u}_i = \mathbf{0}$, meaning that the link C_iB_i is perpendicular to the prismatic joint and the actuation force can't provide force to the link. The more commonly studied case is for det($\mathbf{J}_A$)=0, corresponding to the second kind of singularity, where the moving platform of the mechanism is locally movable even when all the actuated joints are locked [24]. The matrix $(\mathbf{J}_B^{-1}\mathbf{J}_A)$ represents the mapping between the actuation velocity and the output platform velocity and its condition number can represent the kinematic performance. The inverse of the condition number at any configuration is commonly used and its value is between 0 and 1. Here 0 corresponds to the singular configurations, and 1 represents the best mapping. An example is shown in Fig.6 for a constant orientation workspace. It can be seen that the highest performance lies in the area between (x=[-10 : 0] and y=[-23:7] which covers the desired workspace.

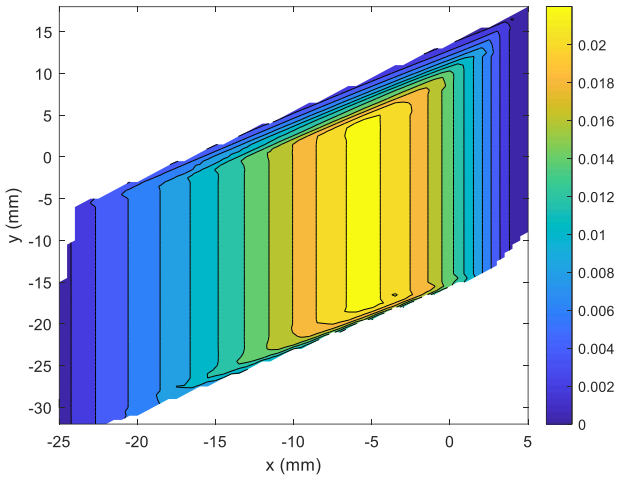

Figure 6 Kinematics performance and singularity-free workspace

3.3 OPTIMIZATION

The objective of the optimization process is to obtain the geometric parameters for the most compact 3-PRR planar parallel mechanism that has the characteristics of the desired workspace. An algorithm to synthesize mechanisms whose workspace is as close as possible to a prescribed workspace, by computing the intersection of the actual and desired workspaces and optimizing it was presented by Gosselin and Guillot [39]. They characterized the desired and actual workspaces by their surface areas and minimized the difference between the surface areas. Merlet [40] presented an algorithm to determine all the possible geometries of 6-DOF parallel mechanisms whose workspace must include a desired workspace described as a set of geometric objects. Murray et al. [41] presented a technique for designing planar parallel mechanisms using planar quaternions that contained any number of prescribed poses as a part of their workspace. Boudreau and Gosselin [42] used a Genetic Algorithmic approach to find geometric parameters of 3-DOF

planar parallel mechanisms, and then determined the intersection between the actual workspace and the prescribed workspace, and minimized the area of the regions that did not intersect. An alternate method to describe the actual and desired workspaces by means of geometric objects was presented in [43], where the author discretized the work space into a grid and the constraints of the problem were evaluated at every grid point of the workspace.

Genetic Algorithms are used to determine optimum structural and geometric parameters of the 3-PRR mechanism in this work. Genetic Algorithm is an optimization method inspired by natural evolution. The fittest members of a population, as identified by their degree of compliance to the objective function (or fitness function), have a better chance of contributing towards the composition of the next generation of the population. This results in good convergence properties of the method towards an optimal solution. In our study, each member of the population consists of vectors that are populated by geometric parameters related to the design of the parallel mechanism. As the algorithm converges towards optimal values, the parameters take values that give a planar parallel mechanism having a workspace as close as possible to the prescribed workspace [29].

The planar platform to be synthesized should have a translational reach of 30 mm along both x-axis and y-axis at zero orientation Ø=0^{o}, and a rotational range of 15^{o} around the frontal plane of the elbow similar to Ref. [35]. We developed an optimization procedure that consists of minimizing the error between the actual and desired workspace for a given mechanism geometry. Since the proposed 3-PRR parallel mechanism has two parallel prismatic joint axes, translation along the y-axis is free and

can be adjusted at any stage to reach the desired translation workspace along this direction. In this case, the desired workspace is focused on the x-direction and described by prescribing a) maximum width along the x-axis of the fixed coordinate frame ($w_{desired}$), and b) maximum range of orientations of moving platform (frame) ($\phi_{desired}$).

In the most general case, the size of the moving platform, the locations and orientations of the base pivots, lengths of the RR-chain connecting the base and the moving platform are all variables, fifteen (15) in total.

$$\boldsymbol{p} = [(x_{A1}, y_{A1}), (x_{A2}, y_{A2}), (x_{A3}, y_{A3}), (x'_{C1}, y'_{C1}), (x'_{C2}, y'_{C2}), (x'_{C3}, y'_{C3}), l_1, l_2, l_3] \quad (17)$$

From the discussion about the specific architecture of the 3- PRR platform that will be used as a self-alignment mechanism, further simplifications can be made . Since we have chosen the shape of the moving and base platform to be rectangular, and for A1 and A3 to lie on the same vertical line (as in Fig. 4a), in the interest of symmetry the distance between A1/A3 and the y-axis is set to be the same as the distance been the y-axis and A2, i.e. ($x_{A1} = -x_{A2} = x_{A3}$). Similar conditions are set for the pivots of the moving platform, i.e. ($x'_{C1} = -x'_{C2} = x'_{C3}$). This reduces the vector of variables to an eleven-element array.

$$\boldsymbol{p}' = [x_{A1}, y_{A1}, y_{A2}, y_{A3}, x'_{C1}, y'_{C1}, y'_{C2}, y_{C3}, l_1, l_2, l_3] \quad (18)$$

For a given geometry of a 3-PRR planar parallel mechanism, we can find the width of its translational workspace at $\phi = 0$ by solving the inverse kinematics problem at set of uniformly distributed discrete points in the desired workspace. The planar parallel

platform can be assembled successfully at all points where ρ_i for i = 1,2,3 are real. Values of $\boldsymbol{p}'$ are generated near the middle of the range during the first run of the genetic algorithm, and in subsequent runs based on the fitness values. The values of ϕ are incremented in steps of 1^0 from -15^0 to $+15^{0.}$ To test if the value of ρ_i calculated at any given point on the desired workspace is real, we assume that it has the following general form:

$$\rho_i = |z_i| (\cos v_i + j \sin v_i) \tag{19}$$

If ρ_i is real-valued:

$$\rho_i \bar{\rho}_i = |z_i|^2 (\cos {v_i}^2 + \sin {v_i}^2) - 1 \neq 0$$

where the argument, $Arg(|z_i|) = 0$ if ρ_i is a real number.

To obtain the parameters of the 3-PRR planar parallel mechanism that has a workspace containing the prescribed workspace, a fitness function is constructed. The fitness function measures the square of the error based on the relative position of the moving platform within the desired workspace, and is mathematically expressed as:

$$F(\boldsymbol{p}', \phi) = \sum_{k=1}^{1000} \sum_{\phi=-15^o}^{15^o} \sum_{i=1}^{3} (|z_i| Arg(|z_i|))^2 \tag{20}$$

where $\boldsymbol{p}'$ is the vector containing the geometric parameters that define the 3-PRR platform. The optimization process was carried out using MATLAB's Genetic Algorithm solver, using default settings, and the algorithm stops after 71 generations with a fitness value of 2.78 after no change in value of the fitness function is detected for successive iterations.

Optimization Constraints

To successfully assemble the 3-PRR planar parallel mechanism, some geometric constraints of the mechanism must be satisfied.

1. Lower and upper bounds must be set for the sizes of the base and moving platforms in the optimization process to yield physically meaningful results.

2. Each chain $B_i\ C_i$ (which represents the length l_i) should have sufficient length to allow the moving platform to reach the edges of the desired workspace, hence lower and upper bounds must be set for l_1,l_2,l_3.

3.4 RESULTS: Optimized Design and Fabrication

The optimization problem is solved using built-in Genetic Algorithm code in MATLAB. The solution of the problem are the following parameters (points A_1, A_2, A_3, y_{c1}, y_{C2}, y_{c3}, and links lengths l_1, l_2, *and* l_3) which are shown in Table 1. Accordingly, the links, base and moving platform of the realized 3-PRR mechanism were fabricated from Aluminum Alloy. Two 130x5x5 mm^3 slider guides with three 19x17x6 mm^3 sliders were mounted on the base as shown in Fig. 7a.

Table 1: Optimized 3-PRR Parameters

A_1	(-52.4, -53.75) mm	C_1'	(-20, -35.36) mm
A_2	(52.4, -34.25) mm	C_2'	(40, 26.42) mm
A_3	(-52.4, 53.75) mm	C_3'	(-20, 8.93) mm
l_1	37.43 mm	α_1	90 degrees
l_2	37.42 mm	α_2	90 degrees
l_3	40.89 mm	α_3	-90 degrees

We performed experimental setup to measure the reachable workspace of the developed 3-PRR mechanism using the OptiTrack system as shown Fig. 7a. Three markers representing the points C1, C2, and C3 are placed at the mechanism to optically track the centroid of the resultant triangle of these markers through the OptiTrack system. Moreover, 6 extra markers are set to calibrate the table horizontal plan with the Optitrack System. It was confirmed that the mechanism was capable to reach from -30.7 mm to 2.9 mm in the x-axis, and -32.1 mm to 54.4 mm in the y-axis. Moreover, despite the irregular shape of the workspace, the mechanism moves smoothly all over its workspace due to the low friction between its links. Referring to Fig. 7-b, the red area represents the reachable workspace with all orientation computed through the theoretical model presented above, while the black area shows the reachable workspace measured through the experimental setup (Fig.7-a). As can be seen that the experimental workspace lies within the theoretical workspace which validates the design and prototype of the mechanism. It's also worthy to highlight that the theoretical workspace covers more area due to the fact that it does not include the physical constraints imposed by different parts of the mechanism like the width of the links and dimensions of the slider bases that affect the workspace as the links collide with each other.

Moreover, the desired constant orientation workspace at φ=0° lies in the yellow box in Fig. 7-b. The asymmetrical workspace can be referred to the selected configuration of parallel prismatic joints. Finally, the realized mechanism would reach more than the desired workspace due to the non-zero orientation reachable points. The extended

workspace in the y-direction is anticipated to be desirable to compensate for the skin deformation due to the interaction between the skin and the exoskeleton.

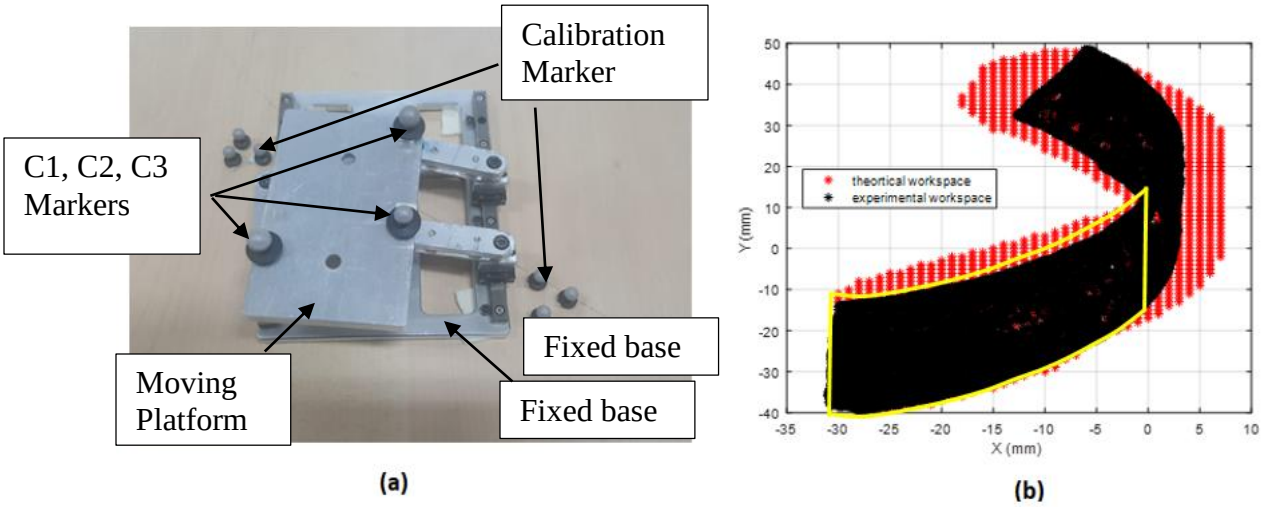

Figure 7: (a) The realized 3-PRR mechanism being prepared for tracking the centroid of the moving platform through optical tracking system. (b) The theoretical (red) and experimental (black) reachable workspace of the 3-PRR mechanism and the desired constant orientation workspace at φ=0^{o} is highlighted in the yellow box.

4 QUANTITATIVE AND QUALITATIVE EXPERIMENTS

4.1 Quantitative Test:

The quantitative test aims to validate the capability of SAE-Exo to perform the axis alignment of its elbow joint with user's elbow. The procedure of this test is inspired by the one presented in [26]. Three healthy male subjects (Age: 30, 32, 33) volunteered to participate in the experiment. Each subject wore SAE-Exo and performed a cyclical flexion extension movement (amplitude of about 100^{o}, frequency of about 0.25 Hz, and total duration of 20 s). The Axis of rotation (A_R) was tracked through an optical tracking system (OptiTrack) using 6-passive optical markers, 3 markers were placed at both sides of the exoskeleton elbow joint. The line that flows between the combinations of the two sets of

markers is the instantaneous axis of revolution of the exoskeleton (A_R). The subject arm was rested on a horizontal table to ensure that there is no change in the z-direction as we are only testing for the changes in x, y and the orientation.

The procedure for each subjects starts by resting the subject's arm on the horizontal table at either the full extension or full flexion posture. Then we record the initial position of the axis of the revolution. Then we track the changes in the position and orientation of the axis of revolution (A_R). A sample of a recorded planar motion of the axis of revolution (A_R) is shown in Fig. 8. A sample of tracking of changes in x, y and orientation (Ø) at the center of the line that represents the axis of revolution is shown in Fig. 9. The readings of both figures correspond to the global Optitrack system reference frame. From Fig. 8 and 9, it can be noticed that the center point of the axis of revolution has traveled a maximum of 18.2 mm in the x-direction, while it covers 78.3 mm in the y-direction. The large span in the y-axis can be related for both the displacement in the joint's y-position and the deformation of the skin due to the interaction with the exoskeleton. Moreover, the span of change in orientation covers around 11 degrees.

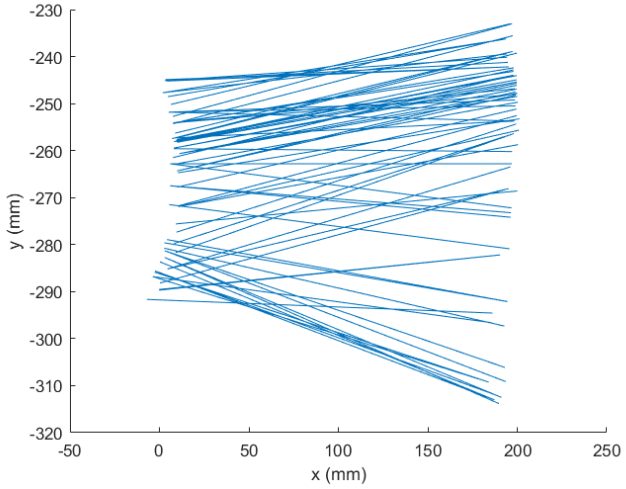

Figure 8: A sample of the tracked Axis of Revolution (A_R) of the SAE-Exo using OptiTrack optical tracking system

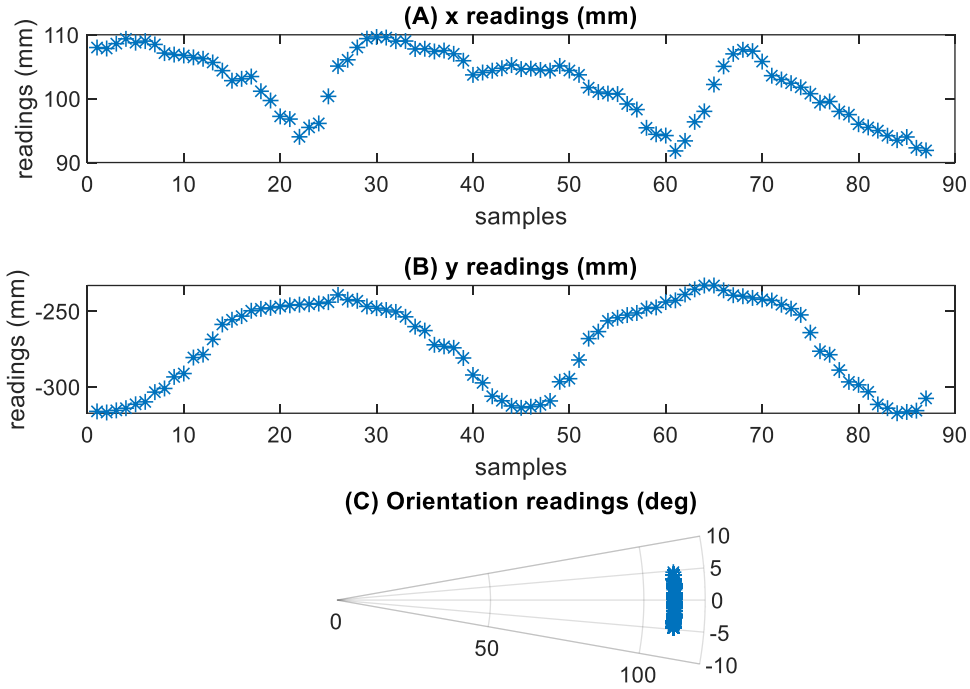

Figure 9: A sample for the tracking of changes in x (A), y (B) and orientation (of the SAE-Exo using OptiTrack optical tracking system).

Table 2 reports the changes (absolute difference between the maximum and minimum values) in the x-direction, y-direction and the orientation for the three subjects. It

Table 2: Results of the characterization of the motion of the axis of revolution of the SAE-Exo

Subject	#1	#2	#3	Mean +STD
$\|\Delta x\|$ (mm)	18.2	18.7	18.4	18.433±0.251
$\|\Delta y\|$ (mm)	78.3	73.1	78.5	76.633±3.06
$\|\Delta \emptyset\|$ (deg)	9.9	10.9	10.2	10.333±0.512

As shown in the results, the changes in x are quite small and approximately within the range of translation motion of the frontal plane of the human elbow [20]. The changes in the y direction are affected by the elasticity of the skin tissues. Thus, the ranges of motion of the exoskeleton exceeded the translational ranges of motion of the frontal plane of the human elbow. The changes in the orientation shows that the exoskeleton has followed the frustum vertex angle of the frontal plane β_f and is inline to the result presented in [26]. However, it is noteworthy to highlight that the ranges of x-motion and orientation in the results have covered only 62.3% and 72.6% respectively of the calculated ranges. This can be related to the restrictions imposed by the current experiment, which limited motion only to the horizontal plane. In the future, an improved test bed to facilitate testing the exoskeleton in more ergonometric way will be utilized.

4.2 Qualitative Test

The qualitative test aims to check the user's opinion on the usefulness and possible concerns related to the designed exoskeleton for performing upper limb

movement while wearing it. Eight healthy users (6 males and 2 females, average age 32.1) were asked to fill the Usefulness-Satisfaction-and-Ease-of use questionnaire [37] that focuses on the experience of the system usage. This questionnaire uses a seven-point Likert rating scale. Mean and standard deviation (SD) of the questionnaire factors are presented in Table 3.

Table 3: Questionnaire factors and relative marks. The mark ranges from "1 = strongly disagree" to "7 = strongly agree". Mean and standard deviation (Mean (SD)) are reported.

Questionnaire factors	**Mean (SD)**
Usefulness	5(0.7)
Ease of use	6.5(0.6)
Ease of learning	6.3(0.7)
Satisfaction	5 (0.6)

Moreover, to evaluate the user's satisfaction to the proposed elbow exoskeleton and its functionality, we asked the users to fill the first part of the QUEST 2.0 questionnaire [38]. The purpose of the QUEST questionnaire is to evaluate how satisfied users are with the proposed assistive device. The mark ranges from "1 = not satisfied at all" to "5 = very satisfied". Mean and standard deviation (Mean (SD)) are reported in Table 4. The results showed the users were satisfied in terms of ergonomics, easy to use and comfort.

Table 4: Quebec User Evaluation of Satisfaction with assistive Technology. The mark ranges from "1 = not satisfied at all" to "5 = very satisfied". Mean and standard deviation (Mean (SD)) are reported.

How satisfied are you with	**Mean (SD)**
the **dimensions** (size, height, length, width) of your assistive device?	4 (0.7)
the **weight** of your assistive device?	4.2(0.6)
how **safe** and **secure** your assistive device is?	4.2(0.8)
the durability (endurance, resistance to wear) of your assistive device?	4 (0.8)
how **easy** it is to use your assistive device?	4.5 (0.7)
how **comfortable** your assistive device is?	4.3(0.7)
how **effective** your assistive device is (the degree to which your device meets your needs)?	4.2(0.8)

5 CONCLUSIONS & FUTURE WORK

In this paper, we presented the double-layered elbow exoskeleton interface with 3-PRR planar parallel mechanism for self-alignment of exoskeleton axes with human anatomical joint axes. A methodology for obtaining the smallest 3-PRR planar parallel mechanism geometry that has the workspace characteristics required for self-alignment of exoskeleton axes at the elbow joint is presented. We solve the optimization problem for a set containing twelve design variables that define the 3-PRR planar parallel mechanism geometry, using Genetic Algorithm.

We performed quantitative and qualitative experiments to validate the capability of SAE-Exo to perform the axis alignment of its elbow joint with user's elbow. Moreover, we obtained user feedback in terms of usefulness and possible concerns related to the designed exoskeleton for performing upper limb movement while wearing it. The results showed general user satisfaction in terms of ease of use, ergonomics, and comfort. The proposed system is a first step towards the realization of self-alignment elbow exoskeleton platform that can be used for rehabilitation and for other clinical needs.

Additional opportunities for the proposed device include patient monitored rehabilitation training that can be done at home and direct ADL assistance. In future, we aim to explore these use case scenarios and to perform detailed experiments on the targeted patients.

ACKNOWLEDGMENT

This work is partially supported by the ADEK Award for Research Excellence (AARE) 2017 with project No.081.

REFERENCES

[1] Go, Alan S. et al. ,2014 , "Heart disease and stroke statistics" , Circulation 129 (3), pp 28-292, https://doi.org/10.1161/01.cir.0000441139.02102.80

[2] Barreca, S, Wolf, , S. L., Fasoli S., and Bohannon R., 2003, "Treatment interventions for the paretic upper limb of stroke survivors: A critical review," Neuro-rehabil. Neural Repair, 17(4), pp. 220–226, DOI: 10.1177/0888439003259415

[3] Volpe, B. T, Krebs, H. I., Hogan N., 2001, " Is robot-aided sensorimotor training in stroke rehabilitation a realistic option?", Current opinion in neurology 14 (6), pp.745-752. https://www.ncbi.nlm.nih.gov/pubmed/11723383

[4] Masiero, S., Celia, A., Rosati, G., and Armani, M., 2007, "Robotic-assisted rehabilitation
of the upper limb after acute stroke", Archives of physical medicine and rehabilitation 88 (2), pp 142-149. DOI: 10.1016/j.apmr.2006.10.032

[5] Chiri A., Vitiello N., Giovacchini, F. Roccella S., Vecchi F., and Carrozza M. C., 2012, "Mechatronic design and characterization of the index finger module of a hand exoskeleton for post-stroke rehabilitation", Mechatronics, IEEE/ASME Transactions on 17 (5) pp 884-894. doi: 10.1109/TMECH.2011.2144614

[6] Kwakkel. G., Kollen B., and H. Krebs, 2007, "Effects of robot-assisted therapy on upper limb recovery after stroke: A systematic review," Neurorehabil. Neural Repair, 22, pp. 111–121. DOI: 10.1177/1545968307305457

[7] Krebs H. I., Hogan N., Aisen M. L., and Volpe B. T., 1998, "Robot-aided neuro rehabilitation," IEEE Trans. Rehabil. Eng. 6(1), pp. 75–87, https://www.ncbi.nlm.nih.gov/pubmed/9535526

[8] Lo A. C., Guarino P. D., Richards L. G., Haselkorn J. K., Wittenberg G. F., Federman D. G., Ringer R. J., Wagner T. H., Krebs H. I., Volpe B. T., Bever C. T., Bravata D. M., Duncan P. W., Corn B. H., Maffucci A. D., Nadeau S. E., Conroy S. S., Powell J. M.,

Huang G. D., and Peduzzi P.,2010, “Robot-assisted therapy for long-term upper-limb impairment after stroke,” New Engl. J. Med., 362, pp. 1772–1783. DOI: 10.1056/NEJMoa0911341

[9] Fasoli S. E., Krebs H. I., Stein J., Frontera W. R., and Hogan N., 2003, “Effects of robotic therapy on motor impairment and recovery in chronic stroke,” Arch. Phys. Med. Rehabil 84(4), pp. 477–482, 2003. DOI:10.1053/apmr.2003.50110

[10] Lum P. S., Burgar C. G., Kenney D. E., and Van der Loos H. F. M., 1999 “Quantification of force abnormalities during passive and active-assisted upper-limb reaching movements in post-stroke hemiparesis,” IEEE Trans. Biomed. Eng.46(6), pp. 652–662, doi: 10.1109/10.764942

[11] Micera S., M. Carrozza C., Guglielmelli E., Cappiello G., Zaccone F., Freschi C., Colombo Mazzone R., A., Del conte C., Pisano F., Minuto G., and Dario P., 2006, “A simple robotic system for neuro-rehabilitation,” J. Auton. Robots 19(3), pp. 271–284. DOI: 10.1007/s10514-005-4749-0

[12] Reinkensmeyer D. J., Takahashi C. D., Timoszyk W. K., Reinkensmeyer A. N., and Kahn L. E., 2001“ Design of robot assistance for arm movement therapy following stroke,” Adv. Robot., 14 (7), pp. 625–637,. /doi.org/10.1163/156855301742058

[13] Mayhew D., Bachrach B., Rymer W., and Beer R., 2005, “Development of the MACARM—A novel cable robot for upper limb neuro rehabilitation,” in Proc. IEEE Int. Conf. Rehabil. Robot., Chicago, IL, Jun./Jul., pp. 299–302. doi: 10.1109/ICORR.2005.1501106

[14] Jia-Fan Z., Can. Jun Y., Ying C., Yu Z., and Yi-Ming D., 2008 “Modeling and control of a curved pneumatic muscle actuator for wearable elbow exoskeleton,” Mechatronics, 18, pp. 448–457,. https://doi.org/10.1016/j.mechatronics.2008.02.006

[15] Perry J. C., Rosen J., and Burns S., 2007, “Upper-limb powered exoskeleton design,” IEEE/ASME Trans. Mechatronics, vol. 12, no. 4, pp. 408–417, doi:10.1109/TMECH.2007.901934

[16] Cempini Marco, De Rossi Stefano MM, Lenzi Tommaso, Vitiello Nicola, and Carrozza Maria. 2013 “Self-alignment mechanisms for assistive wearable robots: A kinetostatic compatibility method. Robotics”, IEEE Transactions on, 29(1), pp236–250, doi: 10.1109/TRO.2012.2226381.

[17] Stienen Arno HA, Hekman Edsko EG, Van Der Helm Frans CT, and Van Der Kooij Herman. 2009 “Self-aligning exoskeleton axes through decoupling of joint rotations and translations.” IEEE Transactions on Robotics, 25(3), pp. 628– 633 doi: 10.1109/TRO.2009.2019147

[18] Dollar, Aaron M and Herr Hugh. 2008 “Lower extremity exoskeletons and active orthoses: challenges and state-of-the-art. Robotics”, IEEE Transactions on, 24(1):144–158, doi: 10.1109/TRO.2008.915453.

[19] Frisoli, Antonio, Rocchi, Fabrizio, Marcheschi, Simone, Dettori, Andrea, Salsedo, Fabio, and Bergamasco, Massimo., 2005, “A new force-feedback arm exoskeleton for haptic interaction in virtual environments.” In Eurohaptics Conference, 2005 and Symposium on Haptic Interfaces for Virtual Environment and Tele-operator Systems, 2005. WorldHaptics2005. First Joint, pp. 195–201. doi: 10.1109/WHC.2005.15

[20] Perry, Joel C, Rosen, Jacob, and Burns, Stephen., 2007, “Upper-limb powered exoskeleton design”. IEEE/ASME transactions on mechatronics, 12(4): pp. 408-417, doi: 10.1109/TMECH.2007.901934

[21] Stienen A. H. A. *et al*., 2007, "Dampace: dynamic force-coordination trainer for the upper extremities," *2007 IEEE 10th International Conference on Rehabilitation Robotics*, Noordwijk, 2007, pp. 820-826. doi: 10.1109/ICORR.2007.4428519

[22] Stienen, Arno HA, Hekman, Edsko EG, Ter Braak, Huub, Arthur MM Aalsma, van der Helm, Frans CT, and van der Kooij, Herman. 2008, “Design of a rotational hydro-elastic actuator for an active upper-extremity rehabilitation exoskeleton”. In Biomedical Robotics and Biomechatronics, 2008. BioRob 2008. 2nd IEEE RAS & EMBS International Conference on, Scottsdale, AZ , pages 881–888., doi: 10.1109/BIOROB.2008.4762873.

[23] Schiele, Andr´e and van der Helm Frans CT., 2006, “Kinematic design to improve ergonomics in human machine interaction”. Neural Systems and Rehabilitation Engineering, IEEE Transactions on, 14(4): pp. 456–469, doi: 10.1109/TNSRE.2006.881565.

[24] Sanchez Jr, RJ, E , Smith Wolbrecht R, Liu J, Rao S, Cramer S, Rahman T, Bobrow JE, and Reinkensmeyer DJ. 2005, “A pneumatic robot for re-training arm movement after stroke: Rationale and mechanical design”. 9*th International Conference on Rehabilitation Robotics, 2005. ICORR 2005.*, Chicago, IL, 2005, pp. 500-504. doi: 10.1109/ICORR.2005.1501151

[25] Nef Tobias, Mihelj Matjaz, and Riener Robert. 2007 , “Armin: a robot for patient-cooperative arm therapy”. Medical & biological engineering & computing, 45(9):887–900, DOI: 10.1007/s11517-007-0226-6.

[26] Vitiello Nicola, Lenzi Tommaso, Roccella Stefano, De Rossi Stefano MM, Cattin Emanuele, Giovacchini Francesco, Vecchi Fabrizio, and Carrozza Maria. 2013, “Neuroexos: A powered elbow exoskeleton for physical rehabilitation”. Robotics, IEEE Transactions on, 29(1): pp. 220–235 doi: 10.1109/TRO.2012.2211492

[27] Jarrasse N. and Morel G., 2012, "Connecting a Human Limb to an Exoskeleton," in *IEEE Transactions on Robotics* 28(3): pp. 697-709, doi: 10.1109/TRO.2011.2178151

[28] Bottlang M, Madey SM, Steyers CM, Marsh JL, Brown TD. 2000, "Assessment of elbow joint kinematics in passive motion by electromagnetic motion tracking." J Orthop Res 18(2): pp. 195-202. DOI:10.1002/jor.1100180206

[29] Ericson A, Arndt A, Stark A, Wretenberg P, Lundberg A., 2003, "Variation in the position and orientation of the elbow flexion axis.", J Bone Joint Surg Br 85(4): pp.538-44, https://www.ncbi.nlm.nih.gov/pubmed/12793560

[30] Bottlang M, Marsh JL, and Brown TD. 1998, "Factors influencing accuracy of screw displacement axis detection with a dc-based electromagnetic tracking system". Journal of biomechanical engineering, 120(3):431–435, https://www.ncbi.nlm.nih.gov/pubmed/10412412 .

[31] Junius, Karen , Degelaen, Marc, Lefeber, Nina, Swinnen, Eva, Vanderborght, Bram and Lefeber, Dirk, 2017, "Bilateral, Misalignment-Compensating, Full-DOF Hip Exoskeleton: Design and Kinematic Validation", Applied Bionics and Biomechanics, 2017, Article ID 5813154, 14 pages, https://doi.org/10.1155/2017/5813154

[32] Duck TR, Dunning CE, King GJ, Johnson JA., 2003, "Variability and repeatability of the flexion axis at the ulnohumeral joint.", J Orthop Res 21(3): pp. 399-404. DOI:10.1016/S0736-0266(02)00198-5

[33] I. A. Kapandji, Fisiologia Articolare—Arto Superiore, Paris, France: Maloine, 2002.

[34] Gosselin, C. M. , Lemieux, S. and Merlet, J., 1996, "A new architecture of planar three-degree-of-freedom parallel manipulator," Proceedings of IEEE International Conference on Robotics and Automation, Minneapolis, MN, USA, 1996, pp. 3738-3743 vol.4. doi: 10.1109/ROBOT.1996.509283

[35] Ghosh S, Gan D. , 2016, "Design of Passive 3-PRR Planar Parallel Manipulators for Self-Alignment of Exoskeleton Axes". ASME. International Design Engineering Technical Conferences and Computers and Information in Engineering Conference, *Volume 5B: 40th Mechanisms and Robotics Conference* , V05BT07A042. doi:10.1115/DETC2016-59821.

[36] Lou, Yunjiang, Liu, Guanfeng, Chen, Ni and Li, Zexiang, 2005, "Optimal design of parallel manipulators for maximum effective regular workspace," *2005 IEEE/RSJ International Conference on Intelligent Robots and Systems*, Edmonton, Alta., 2005, pp. 795-800. doi: 10.1109/IROS.2005.1545144

[37] Lund, A. M. , 2001, "Measuring usability with the use questionnaire". Usability interface,2001.8(2):3–6. (www.stcsig.org/usability/newsletter/index.html)

[38] Demers, L., Weiss-Lambrou, R., and Ska, B. 2002. "The Quebec user evaluation of satisfaction with assistive technology (quest 2.0): an overview and recent progress".

Technology and Disability, 14(3):101–105. https://www.semanticscholar.org/paper/The-Quebec-User-Evaluation-of-Satisfaction-with-(-2-Demers-Weiss-Lambrou/ae5a8507a9ecd4ac567be7904f51437daee571bf

[39] Gosselin, Clement M and Guillot, Michel, 1991 "The synthesis of manipulators with prescribed workspace". Journal of Mechanical Design, 113(4):451–455, 1991. doi:10.1115/1.2912804

[40] Merlet J.P. 1997, "Designing a parallel manipulator for a specific workspace." the International Journal of Robotics research, 16(4):545–556,. https://doi.org/10.1177/027836499701600407

[41] Murray Andrew P, Pierrot ,Francois, Dauchez, Pierre, and McCarthy, J Michael, 1997. "A planar quaternion approach to the kinematic synthesis of a parallel manipulator." Robotica, 15(04):361–365, https://doi.org/10.1017/S0263574797000441 .

[42] Boudreau Roger and Gosselin CM. 1999, "The synthesis of planar parallel manipulators with a genetic algorithm." Journal of Mechanical Design, 121(4):533–537,. doi:10.1115/1.2829494

[43] S Caro, D Chablat, R Ur-Rehman, and P Wenger. Multiobjective design optimization of 3–prr planar parallel manipulators. In Global Product Development, pages 373–383. DOI https://doi.org/10.1007/978-3-642-15973-2_37

[44] Li, J., Cao, Q., Zhang, C., Tao, C., & Ji, R. (2019). Position solution of a novel four-DOFs self-aligning exoskeleton mechanism for upper limb rehabilitation. *Mechanism and Machine Theory*, *141*, 14-39.

[45] Wu, K. Y., Su, Y. Y., Yu, Y. L., Lin, C. H., & Lan, C. C. (2019). A 5-Degrees-of-Freedom Lightweight Elbow-Wrist Exoskeleton for Forearm Fine-Motion Rehabilitation. *IEEE/ASME Transactions on Mechatronics*.

[46] Wang, J., Li, X., Huang, T. H., Yu, S., Li, Y., Chen, T., ... & Su, H. (2018). Comfort-centered design of a lightweight and backdrivable knee exoskeleton. *IEEE Robotics and Automation Letters*, *3*(4), 4265-4272.

APPENDIX A: GENERAL ARCHITECTURE AND KINEMATICS MODEL

The planar 3-PRR parallel mechanism is a three DOF parallel mechanism consisting of three kinematic chains. Each chain consists of a prismatic joint fixed to the base, followed by two revolute joints. As originally proposed in [34], the general architecture of the 3-PRR chain is shown in Fig.A1. Two coordinates are used to determine the relative motion between the fixed base and the moving platform. The fixed base lies on the global coordinate O_{xy} and the centroid of the moving platform is the origin of the second

coordinate C (x_0, y_0). The three passive prismatic joints are fixed to the base, located at point Ai with coordinates (x_{Ai}, y_{Ai}) for and its axis of motion is pointed in a direction defined by fixed angle α_i; (i =1, 2 and 3) from the horizontal.

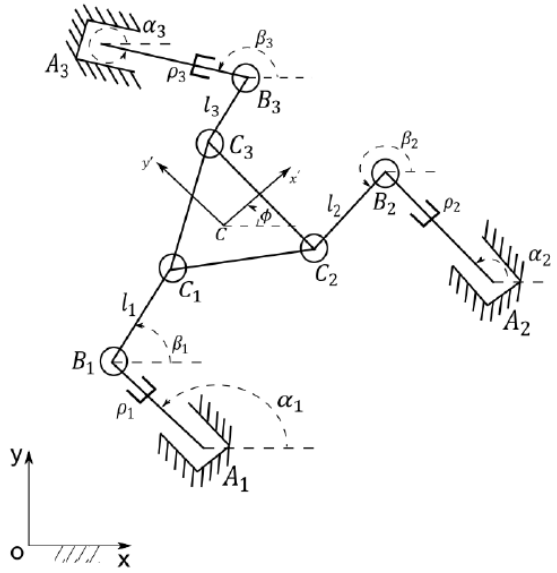

Figure A1: General architecture of a 3-PRR planar parallel mechanism [34]

The moving part of the *i*th unactuated prismatic joint (represented by point B_i) forms a linear displacement from point A_i (x_{Ai}, y_{Ai}). This displacement is defined as ρ_i, (*i* =1, 2 and 3). On the points B_i (*i* =1, 2 and 3), three unactuated revolute joints are located. Three rigid links are connected from these points to the moving platform through points C_i, (i =1, 2 and 3). The lengths of these links are defined as l_i (*i* =1, 2 and 3). The angles formed between the global x-coordinate and the ith link is defined as β_i (*i* =1, 2 and 3). The Cartesian coordinate vector of the mechanism is given by the position and orientation of the platform and can be written as:

$$C = [x_c \;\; y_c \;\; \emptyset] \qquad \text{(A1)}$$

where x_c, y_c are the position coordinates of the platform centroid point C in the global frame. Ø is the angle between the moving coordinate (x',y') and the global frame (x,y).

From Fig. 4, if the position of the sliders, and the orientation of the links are known the three points of the moving platform (C_1, C_2 and C_3) can be expressed as

$$x_{Ci} = x_{Ai} + \rho_i \cos(\alpha_i) + l_i \cos(\beta_i) \quad \text{(A2)}$$

$$y_{Ci} = y_{Ai} + \rho_i \sin(\alpha_i) + l_i \sin(\beta_i) \quad \text{(A3)}$$

Eliminating β_i by using the equation (A2-A3), an expression for ρ_i can be written as follows:

$$\rho_i = (x_{Ci} - x_{Ai}) \cos(\alpha_i) + (y_{Ci} - y_{Ai}) \sin(\alpha_i) \pm \sqrt{l_i^2 + \left((-x_{Ci} + x_{Ai}) \cos(\alpha_i) + (-y_{Ci} + y_{Ai}) \sin(\alpha_i)\right)^2 - (-x_{Ci} + x_{Ai})^2 - (-y_{Ci} + y_{Ai})^2} \quad \text{(A4)}$$

Thus we can obtain a closed form solution to the inverse kinematics problem for a 3-PRR planar platform where real valued sets of ρ_i (i=1,2, and 3) correspond to valid configurations of the planar mechanism.

Further, if the moving platform position and orientation are known the three points of the moving platform (C_1, C_2 and C_3) can also be expressed as:

$$x_{Ci} = x_C + x'_{ci} \cos(\emptyset) - y'_{ci} \sin(\emptyset) \quad \text{(A5)}$$

$$y_{Ci} = y_C + y'_{ci} \cos(\emptyset) + x'_{ci} \sin(\emptyset) \quad \text{(A6)}$$

where x'_{ci}, y'_{ci} are the coordinates of point C_i in the moving frame.

Substituting equations (A5-A6) in (A4), we obtain:

$$\rho_i = \left(x_C - x_{A_i}\right)\cos\alpha_i + x'_{c_i}\cos(\alpha_i - \phi) + y'_{c_i}\sin(\alpha_i - \phi) + \left(y_C - y_{A_i}\right)\sin\alpha_i \pm$$

$$\sqrt{\begin{array}{c} 2\left(x'_{C_i}\left(x_{A_i} - x_C\right) + y'_{C_i}\left(y_{A_i} - y_C\right)\right)\cos\phi \\ +2\left(x'_{C_i}\left(y_{A_i} - y_C\right) - y'_{C_i}\left(x_{A_i} - x_C\right)\right)\sin\phi \\ +\left(\left(x_C - x_{A_i}\right)\cos\alpha_i + \left(y_C - y_{A_i}\right)\sin\alpha_i + x'_{C_i}\cos(\alpha_i - \phi) + y'_{c_i}\sin(\alpha_i - \phi)\right)^2 \\ +l_i^2 - \left(x_C - x_{A_i}\right)^2 - \left(y_C - y_{A_i}\right)^2 - {x'_{C_i}}^2 - {y'_{c_i}}^2 \end{array}} \quad \text{(A7)}$$

Such that the closed form inverse kinematics solution for the 3-PRR planar parallel platform can be obtained if the position and orientation of the mobile platform is known. The closed form inverse kinematics solution thus expressed using the positions of the points C1, C2, C3 in the moving platform reference frame, which is a more intuitive frame for expressing the positions of points on the moving platform.

Figure Captions List

Figure 1 CAD model of the SAE Exo. The main parts of the exoskeletons are labelled in the figure

Figure 2 The complete prototypes of the proposed exoskeleton. It is based parallel planar mechnism for the elbow axis alignment

Figure 3 Anatomy of the human elbow. (1) Humerus. (2) Radius. (3) Ulna. (4) Capitellum. (5) Trochlea. (6) Lateral facet of capitellum. (7) Lateral facet of trochlea. AH is the humerus longitudinal axis, AU is the ulna longitudinal axis, AML is the anatomical medial-lateral

axis passing from the capitellum center to the trochlear center [17],and βh andβf are the frustum vertex angles, respectively, on the horizontal and frontal planes (adopted from [26, 33]) .

Figure 4 (a)Scheme of the realized 3PRR manipulator (b) CAD Model of the 3PRR manipulator

Figure 5 Sample constant orientation workspace (area covered in cyan) of the 3-PRR (a) φ=-10^o, (b) φ=0^o, (c) φ=10^o

Figure 6 Kinematics performance and singularity-free workspace

Figure 7 a) The realized 3-PRR mechanism being prepared for tracking the centroid of the moving platform through optical tracking system. (b) The theoretical (red) and experimental (black) workspace of the 3-PRR mechanism and the desired planar workspace at 0 orientation is highlighted in the yellow box.

Figure 8 A sample of the tracked Axis of Revolution (A_R) of the SAE-Exo using OptiTrack optical

Figure 9 A sample for the tracking of changes in x (A), y (B) and orientation (of the SAE-Exo using OptiTrack optical tracking system).

Figure A1 General architecture of a 3-PRR planar parallel manipulator [34]

Table Caption List

Table 1 Fabricated 3PRR Parameters

Table 2 Results of the characterization of the motion of the axis of revolution of the SAE-Exo

Table 3 Questionnaire factors and relative marks. The mark ranges from “1 = strongly disagree” to “7 = strongly agree”. Mean and standard deviation (Mean (SD)) are reported.

Table 4 Quebec User Evaluation of Satisfaction with assistive Technology. The mark ranges from “1 = not satisfied at all” to “5 = very satisfied”. Mean and standard deviation (Mean (SD)) are reported.